ARTICLE

Nitrogen- and Boron-Doped Double-Walled Carbon Nanotubes

L. S. Panchakarla, A. Govindaraj, and C. N. R. Rao*

Chemistry and Physics of Materials Unit, CSIR Center of Excellence in Chemistry and DST Unit on Nanoscience, Jawaharlal Nehru Centre for Advanced Scientific Research, Jakkur P.O., Bangalore 560 064, India

ABSTRACT Double-walled carbon nanotubes (DWNTs) doped with nitrogen and boron have been prepared by the decomposition of a CH_4 + Ar mixture along with pyridine (or NH_3) and diborane, respectively, over a $Mo_{0.1}Fe_{0.9}Mg_{13}O$ catalyst, prepared by the combustion route. The doped DWNTs bave been characterized by transmission electron microscopy (TEM), X-ray photoelectron spectroscopy, electron energy loss spectroscopy, and Raman spectroscopy. The dopant concentration is around 1 atom % for both boron and nitrogen. The radial breathing modes in the Raman spectra have been employed along with TEM to obtain the inner and outer diameters of the DWNTs. The diameter ranges for the undoped, N-doped (pyridine), N-doped (NH_3), and B-doped DWNTs are 0.73–2.20, 0.74–2.30, 0.73–2.32, and 0.74–2.36 nm, respectively, the boron-doped DWNTs giving rise to a high proportion of the large diameter DWNTs. Besides affecting the G-band in the Raman spectra, N- and B-doping affect the proportion of semiconducting nanotubes.

KEYWORDS: carbon nanotubes · doped nanotubes · double-walled nanotubes · Raman spectroscopy · transmission electron microscopy

Double-walled carbon nanotubes (DWNTs), first observed in 1996, constitute a unique family of carbon nanotubes (CNTs).[1,2] DWNTs occupy a position between the single-walled carbon nanotubes (SWNTs) and the multiwalled carbon nanotubes (MWNTs), as they consist of two concentric cylinders of rolled graphene. DWNTs possess useful electrical and mechanical properties with potential applications. Thus, DWNTs and SWNTs have similar threshold voltages in field electron emission, but the DWNTs exhibit longer lifetimes.[3] Unlike SWNTs, which get modified structurally and electronically upon functionalization, chemical functionalization of DWNTs surfaces would lead to novel carbon nanotube materials where the inner tubes are intact. The stability of DWNTs is controlled by the spacing of the inner and outer layers but not by the chirality of the tubes;[4] therefore, one obtains a mixture of DWNTs with varying diameters and chirality indices of the inner and outer tubes. DWNTs have been prepared by several techniques, such as arc discharge[5] and chemical vapor deposition (CVD) using a mixture of ferrocene with a hydrocarbon or alcohol (typical hydrocarbons are methane, alcohol, *n*-hexane, and benzene).[6–10] DWNTs have also been prepared by a sulfur-assisted CVD method using methane as the carbon source.[11,12]

Applications of CNTs based on their electrical properties strongly depend on the diameter and helicity as well as parity.[2,13] Doping of CNTs by boron and nitrogen renders them p-type and n-type, respectively. MWNTs and SWNTs doped with nitrogen[14–17] and boron[18,19] have been reported. Boron-doped carbon nanotubes appear to exhibit enhanced electron field emission due to the presence of the boron atom at the nanotube edges.[20,21] N-doped CNTs show n-type behavior regardless of tube chirality.[22]

We were interested in the synthesis and characterization of boron- and nitrogen-doped DWNTs in view of their potential applications. We have focused on the low-doping regime (~1 atom %), where the fundamental band structure is expected to be unchanged relative to the all-carbon model. To our knowledge, except for a report on the preparation of nitrogen-doped DWNTs by using a mixture of methane, ammonia, and argon over an iron−molybdenum catalyst,[23] there has been no detailed study of these materials. We have prepared nitrogen-doped DWNTs by the thermal decomposition of a CH_4 + NH_3 + Ar mixture as well as a CH_4 + pyridine + Ar mixture over a $Mo_{0.1}Fe_{0.9}Mg_{13}O$ catalyst, prepared by a new procedure. It may be noted that pyridine has been found to be a good nitrogen source to prepare N-doped MWNTs.[16] We have prepared boron-doped DWNTs by the thermal decomposition of a CH_4 + B_2H_6 + Ar mixture over the $Mo_{0.1}Fe_{0.9}Mg_{13}O$ catalyst at 950 °C.

*Address correspondence to cnrrao@jncasr.ac.in.

Received for review September 13, 2007 and accepted November 01, 2007.

Published online November 29, 2007. 10.1021/nn700230n CCC: $37.00

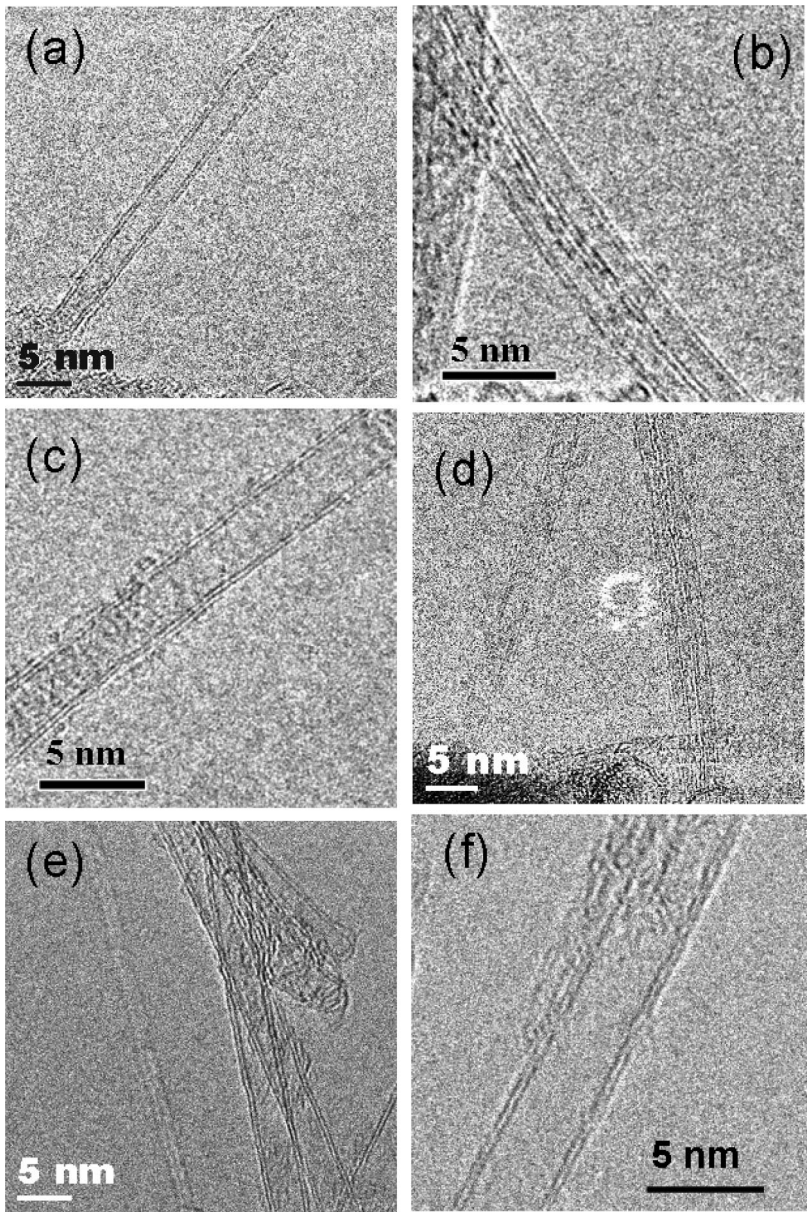

Figure 1. HRTEM images of (a,b) undoped DWNTs, (c) N-doped DWNTs using ammonia, (d) N-doped DWNTs using pyridine, and (e,f) of B-doped DWNTs.

The various DWNTs have been characterized with respect to composition and structure. In particular, the effect of B- and N-doping on the dimensions of the nanotubes has been examined by Raman spectroscopy.

RESULTS AND DISCUSSION

While the decomposition of the CH_4 + Ar over the $Mo_{0.1}Fe_{0.9}Mg_{13}O$ catalyst at 950 °C yielded undoped DWNTs, decomposition of the CH_4 + NH_3 + Ar and CH_4 + pyridine + Ar mixtures gave nitrogen-doped DWNTs. Decomposition of the CH_4 + BH_3 + Ar mixture over the catalyst at 950 °C yielded boron-doped DWNTs. The N- and B-doped DWNTs could not be produced at temperatures lower than 950 °C. The combustion method employed for the preparation of the catalyst seems to help in producing DWNTs exclusively with only a very small or negligible proportion of SWNTs.

We have used both transmission electron microscopy (TEM) and Raman spectroscopy to characterize the different DWNTs samples. TEM allows direct imaging of the DWNTs and gives indications for the presence of other species along with the DWNTs. In the TEM images, we seldom encountered SWNTs or MWNTs. Besides providing information on the nature and dimensions of DWNTs, Raman spectroscopy helps to characterize the purity and quality of the DWNTs. Electron energy loss spectroscopy (EELS), carried out in a high-resolution electron microscope, and X-ray photoelectron microscopy have been employed to determine the elemental composition of the DWNTs.

Undoped DWNTs obtained by us generally had outer tube diameters of 2.2−2.8 nm and inner tube diameters of 1.4−2.1 nm, as shown by the high-resolution TEM (HRTEM) images in Figure 1a,b. In Figure 1c,d, we show typical HRTEM images of purified nitrogen-doped DWNTs synthesized by using NH_3 and pyridine as the nitrogen source, respectively. In Figure 1e,f we show HRTEM images of the boron-doped DWNTs. The HRTEM images indicate that the purified samples of the DWNTs have well-resolved walls and that most of the amorphous carbon was eliminated from the surface during the purification process. HRTEM images reveal that the outer tube diameters of the N-doped DWNTs prepared by using NH_3 as the nitrogen source are in the 1.7–3.2 nm range and the inner tube diameters are in the 1–2.4 nm range. The interlayer spacing is around 0.38 nm. In the case of N-doped DWNTs prepared by using pyridine as the nitrogen source, the outer tube diameters are generally in the 1.6–2.6 nm range, while the inner tube diameters are in the 0.9–1.8 nm range. The interlayer spacing ranges from 0.34 to 0.41 nm. From the HRTEM studies, we surmise that the diameters of the N-doped DWNTs obtained by using pyri-

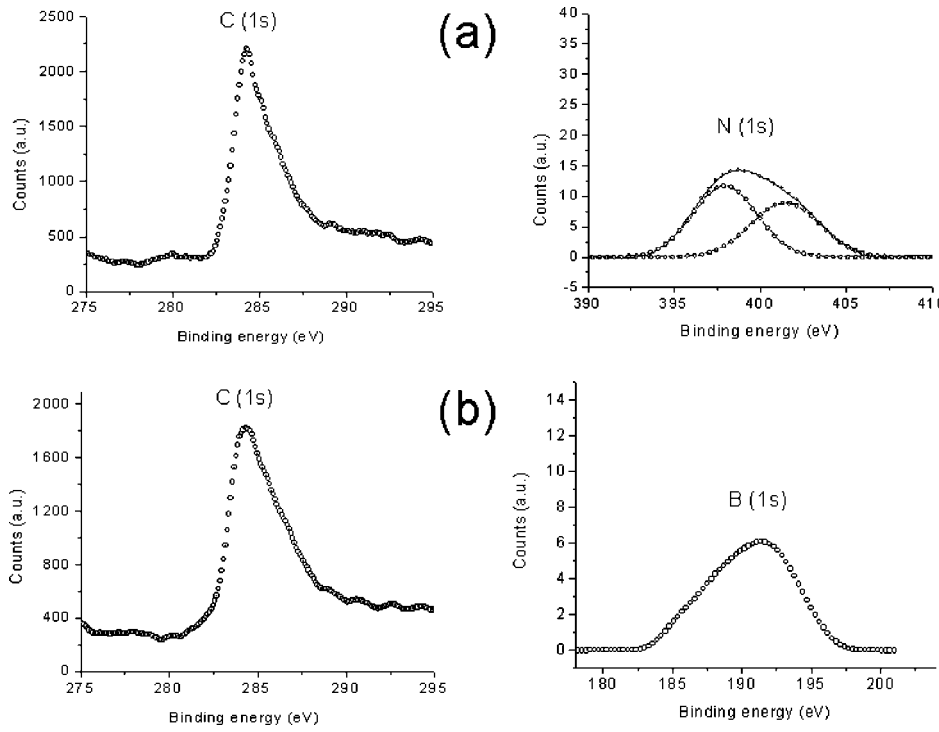

Figure 2. (a) C 1s and N 1s XPS signals of N-doped DWNTs prepared using ammonia. (b) C 1s and B 1s signals of B-doped DWNTs.

dine are smaller than those obtained with NH_3. Thus, the diameters of the N-doped DWNTs appear to depend on the nitrogen source and the reaction conditions employed.

HRTEM images of the boron-doped DWNTs show that they possess larger diameters than the undoped DWNTs as well as the N-doped DWNTs (Figure 1e,f). The outer tube diameters of the B-doped DWNTs range from 2.5 to 4.7 nm, and the inner tube diameters are in the 1.8–3.9 nm range. The interlayer spacing ranges from 0.35 to 0.41 nm. Figure 1f shows the HRTEM image of a large diameter B-doped DWNT with an outer diameter of 4.7 nm and an inner diameter of 3.9 nm.

It has been reported in the literature that boron and nitrogen are incorporated to SWNTs to a smaller extent than in MWNTs.[14–19] We have estimated the compositions of the N- and B-doped DWNTs prepared by us by employing X-ray photoelectron spectroscopy. A core-level X-ray photoelectron spectrumf the N-doped DWNTs obtained by using NH_3 as the N-source is shown in Figure 2a. The C 1s signal is at 284.3 eV, while the N 1s signal is centered at 399.6 eV, indicating of nitrogen substitution in the graphene sheet. It is possible that there is a small amount of amorphous carbon, as suggested by the asymmetry of the C 1s signal, although most of it gets removed on treatment with hydrogen (see Experimental Section). The asymmetric shape of the N 1s peak indicates the existence of at least two components and could be deconvoluted into two peaks at 398 and 401.3 eV. The 398 eV feature is characteristic of pyridinic nitrogen (sp^2 hybridization), while the peak centered at 401.3 eV is due to nitrogen present in graphene sheets.[15] The areas of the two bands bear a ratio of 1:1. On the basis of the total N 1s and C 1s intensities, the nitrogen-to-carbon ratio in the nanotubes samples was calculated by taking the photoionization cross sections of the 1s levels into account. The average composition was thus found to correspond to 1.3 atom % nitrogen. This value is lower than that reported in the literature for DWNTs (~2.9 atom %)[13] and MWNTs (3–10 atom %).[16] The N 1s spectrum of N-doped DWNTs obtained by using pyridine as the nitrogen source shows mainly the band at 398 eV, the intensity of the 401.3 eV band being very small. Thus, there is an intrinsic difference in the nature of N-substitution between the N-doped DWNTs prepared by using NH_3 and pyridine.

Figure 2b shows the core-level spectra of the B-doped DWNTs. The B 1s feature is at 191.4 eV, and the C 1s signal is at 284.3 eV. The shift of the B 1s signal toward higher binding energy compared to that of pure boron (188 eV) indicates that boron is in the sp^2 carbon network. The slight asymmetry of the B 1s signal would, however, suggest the presence of another possible mode of substitution. The boron content works out to be 1 atom %. Around 3 atom % B-doped MWNTs have been reported.[18] EELS measurements in a high-resolution electron microscope confirmed the presence of nitrogen as well as boron in the respective doped DWNTs. The %B and %N were found to be small (~1 atom %), consistent with the XPS data.

The resonance Raman spectrum of DWNTs shows three main features: the G band, the D band, and bands due to the radial breathing modes (RBMs). The tangential stretch G-band modes are in the 1550–1600 cm^{-1} range. The disorder-induced D-band is observed between 1200 and 1450 cm^{-1}. The D-band is activated in the first-order scattering process by the presence of in-plane substitutional heteroatoms, vacancies, grain boundaries, or other defects and by finite size effects, all of which lower the crystalline symmetry of the quasi-infinite lattice.[24] RBM frequencies provide information about the nanotube diameter in the case of SWNTS and DWNTs. We have recorded the Raman spectra of the undoped as well as the N- and B-doped DWNTs by using 632.8 nm excitation using a He−Ne laser. The spectra were collected in a backscattering geometry at room

TABLE 1. RBM Frequencies (cm^{-1}) and Diameter (in Parentheses, nm) of Undoped and N- and B-Doped DWNTs

DWNTs[a]	N-DWNTs (Py)[b]	N-DWNTs (NH_3)[c]	B-DWNTs[d]
338 (0.73)	337 (0.74)	334 (0.73)	336 (0.74)
252 (0.98)	241 (1.03)	308 (0.81)	217 (1.14)*
213 (1.16)*	220 (1.13)*	281 (0.88)	201 (1.23)**
199 (1.25)	214 (1.16)*	247 (1.0)	189 (1.31)**
189 (1.31)*	191 (1.30)	213 (1.16)**	177 (1.40)
175 (1.42)	160 (1.55)**	199 (1.25)	163 (1.52)
171 (1.45)	142 (1.75)**	191 (1.30)	151 (1.64)*
158 (1.57)**	134 (1.85)	158 (1.57)*	130 (1.91)**
143 (1.73)**	125 (1.98)	152 (1.63)**	118 (2.10)*
132 (1.88)**	118 (2.10)	147 (1.69)**	105 (2.36)
113 (2.20)	108 (2.30)	134 (1.85)	
		107 (2.32)	

[a]Possible (*n*,*m*) values for the intense bands are as follows: 213 [(7,10)], 189 [(3,15); (6,13)], 158 [(14,9); (19,2)], 143 [(17,8)], 132 [(18,9); (21,5)]. [b]Possible (*n*,*m*) values for the intense bands are as follows: 220 [(4,12)], 214 [(7,10)], 160 [(18,3); (6,16)], 142 [(20,4); (7,18)]. [c]Possible (*n*,*m*) values for the intense bands are as follows: 213 [(7,10)], 158 [(7,10)], 152 [(13,11); (12,12)], 147 [(21,1); (6,18)]. [d]Possible (*n*,*m*) values for the intense bands are as follows: 217 [(1,14)], 201 [(3,14); (7,11)], 189 [(3,15)], 151 [(18,5); (15,9)], 130 [(16,12)], 118 [(5,24); (15,16)]. *Highest intensity RBM frequency. **Medium intensity RBM frequency.

temperature. Figure 3a shows the G-bands of the pure as well as doped DWNTs. The G-band of the N-doped DWNTs (Py) appears at a lower frequency (1574 cm^{-1}) compared to that of undoped DWNTs (1575 cm^{-1}), whereas the G-band of the B-doped DWNTs appears at a higher frequency (1579 cm^{-1}). The G-band of the N-doped DWNTs (NH_3) also appears at a lower frequency (1571 cm^{-1}). Thus, the shifts of the G-band are opposite for n- and p-doping of the DWNTs. Such shifts of the G-band have been reported for B- and N-doped SWNTs by Yang *et al.*[25] and McGuire *et al.*[26] The small-intensity shoulder around 1540 cm^{-1} seen in the spectra of undoped DWNTs shows a decrease in intensity in the N-doped DWNTs and is negligible in the case of B-doped DWNTs. This band is related to the metallic nature of the nanotubes,[27] and its near absence in N- and B-doped DWNTs suggests a greater prevalence of semiconducting nanotubes. The inset in Figure 3a shows that the intensity of the D-band is high in the case of the B-doped DWNTs and low in the case of the N-doped DWNTs. The *I*(D)/*I*(G) ratios are 0.04, 0.06, and 0.16 for undoped, N-doped (py), and B-doped DWNTs respectively.

We observe several RBM bands in the DWNTs (Figure 3b), resulting from various sizes of the nanotubes, just as in earlier reports.[28] By using the relation $\omega = 248/d$, where ω is the RBM frequency in cm^{-1} and d is the nanotube diameter in nm, we have obtained the diameters of the DWNTs.[28] The RBM frequencies and the corresponding diameters are tabulated in Table 1 for undoped as well as N- and B-doped DWNTs, along with (*n*,*m*) indices for the intense features. From the table, we see that the diameter distribution of the nanotubes is markedly affected by N- and B-doping. The undoped DWNTs show the highest intensity RBM bands centered at 213 and 189 cm^{-1}, corresponding to diameters of 1.16 and 1.31 nm, respectively. The slightly lower intensity or medium-intensity RBM bands are at 158, 143, and 132 cm^{-1}, corresponding respectively to diameters of 1.57, 1.73, and 1.88 nm. The N-doped DWNTs (Py) show the highest intensity RBM bands centered at 220 and 214 cm^{-1}, corresponding to diameters of 1.13 and 1.16 nm, respectively. The slightly lower intensity bands centered at 160 and 142 cm^{-1} correspond to 1.55 and 1.75 nm diameters, respectively. The diameters of the N-doped DWNTs (Py) are somewhat smaller compared to those of the undoped DWNTs. This is, however, not the case with N-doped DWNTs prepared using NH_3 as the nitrogen source. The DWNTs (NH_3) show the highest intensity RBM band at 158 cm^{-1}, corresponding to a diameter of 1.57 nm. The slightly lower intensity bands centered at 213, 152, and 147 cm^{-1} correspond to diameters of 1.16, 1.63, and 1.69 nm, respectively. Since the nature of

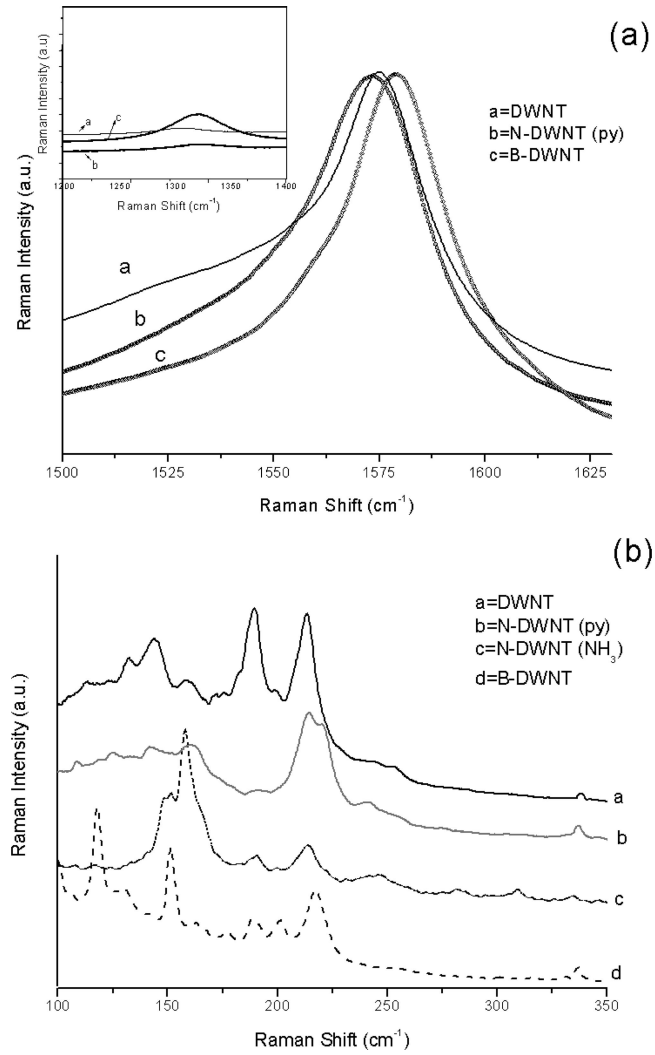

Figure 3. (a) G-bands in the Raman spectra of undoped and doped DWNTs. Inset shows the D-bands of the same. (b) RBM bands of undoped and doped DWNTs.

N-substitution as well as the nature of the defects is different in the N-doped DWNTs prepared by using NH_3 and pyridine, the difference in diameters is not entirely surprising.

The B-doped DWNTs exhibit a high proportion of large-diameter DWNTs compared to the undoped or N-doped DWNTs. The most intense RBM bands of the B-doped DWNTs are at 217, 151, and 118 cm^{-1}, corresponding to diameters of 1.14, 1.64, and 2.1 nm, respectively. The slightly lower intensity bands centered at 201, 189, and 130 cm^{-1} correspond to diameters of 1.23, 1.31, and 1.91 nm, respectively. Due to a cutoff filter, the peaks below 100 cm^{-1} were not detected.

The diameters of the various DWNTs calculated from the RBM modes are comparable with those obtained from the TEM images, but the larger diameter nanotubes seen in the TEM images are not registered in the Raman spectra since the RBM modes below 100 cm^{-1} could not be recorded by us. We can identify DWNT pairs by taking the difference between the inner and outer diameters to be around 0.7 nm. The frequencies (cm^{-1}) of such pairs of the RBM bands in the case of undoped DWNTs are (252,143), (213,132), and (189,113). The metallic (m) and semiconducting (s) natures of these pairs are respectively (s,m), (m,m) or (m,s), and (m,s) or (s,s). In the N-doped DWNTs (py), the pairs are (241,142), (214,125), (220,134), and (160,108), and they are (s,s), (m,s), (s,s), and (m,m) or (m,s), respectively. For N-doped DWNTs (NH_3), the pairs are (281,158), (247,147), (213,134), and (152,107), and these pairs are respectively (s,s), (s,s) or (s,m), (m,s), and (m,m) or (m,s) or (s,m) or (s,s). In the B-doped DWNTs, the pairs are (217,130), (177,118), (189,118), and (151,105), and these pairs are (s,s), (m,s) or (s,s), (m,s), and (m,m) or (m,s) or (s,m) or (s,s), respectively. Taking the semiconducting and metallic nature of all the RBM bands, the ratio of semiconductor to metallic nanotubes in the case of undoped DWNTs works out to be 2:1, while it is 2:1, 2.2:1, and 2:1, respectively, in the case of N-doped DWNTs (py), N-doped DWNTs (NH_3), and B-doped DWNTs. Thus, the RBM modes predict a greater proportion of semiconducting nanotubes in the doped DWNTs as well.

The electronic absorption spectra of undoped as well as doped DWNTs show bands in the 900–1200 nm region due overlapping E_{22}^{s} (s = semiconductor) features of the outer tubes and E_{11}^{S} of inner tubes.[29] The absorption bands in the 1600–2400 nm regions are due to E_{11}^{S} of the outer tubes. The absorption bands due to E_{11}^{m} (m = metal) of the outer tubes are found in the 400–600 nm region. The metallic feature seems to prominent in the undoped DWNTs. Accordingly, the 1540 cm^{-1} G^{+}-band in the Raman spectrum is less prominent in the doped nanotubes.

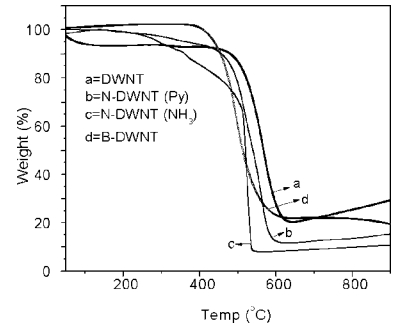

Figure 4. TGA curves of undoped and doped DWNTs.

The smaller diameter carbon nanotubes are known to be less stable than their larger diameter counterparts and tend to oxidize at lower temperatures. Amorphous carbon and carbon nanotubes with defects undergo combustion at lower temperatures. In Figure 4, we show the thermogravimetric analysis (TGA) curves of undoped as well as N- and B-doped DWNTs. The decomposition temperatures of all these doped DWNTs are comparable to but slightly lower that the decomposition temperature of pure DWNTs. Derivative TGA curves also shows the same trend. The slight increase in mass at high temperature may be due to the small metallic impurity.

CONCLUSION

In conclusion, the $Mo_{0.1}Fe_{0.9}Mg_{13}O$ catalyst prepared by the combustion route preferentially yields DWNTs, the proportion of SWNTs being very small or negligible. The use of this catalyst has enabled the synthesis of 1 atom % N- and B-doped DWNTs. The diameters of the nanotubes obtained from the Raman RBM modes and transmission electron microscopy are comparable. The N-doped nanotubes show the G-band in the Raman spectrum at a lower frequency than the undoped ones, while the B-doped nanotubes show an increase in the frequency. The proportion of the metallic nanotubes appears to decrease on N- or B-doping, but the average diameter is substantially larger in the B-doped DWNTs.

EXPERIMENTAL SECTION

Synthesis of DWNTs was carried out in a quartz tube reactor. For each synthesis, 200 mg of the supported Fe−Mo catalyst (Fe−Mo/MgO) was placed in a quartz boat by spreading it uniformly. The quartz boat was inserted into the center of the quartz tube (25 mm i.d. and 1 m long) mounted inside an electrical tube furnace. Subsequently, the furnace was heated to 950 °C in an argon atmosphere at a heating rate of 3 °C/min. A mixture of methane and Ar gas was introduced into the reactor. The flow rates of methane and Ar were maintained at 50 and 150 sccm (standard cubic centimeters per minute), respectively. After 20 min, the reactor was cooled to room temperature in an Ar atmosphere. The resulting black dense mat contained a homogeneous dispersion of carbon nanotubes around the oxide grains. This crude material was carefully collected from the boat and subjected to purification.

The oxide precursors required to prepare the catalyst for the synthesis of DWNTs were prepared by the combustion

route.[30,31] The required amount of $(NH_4)_6Mo_7O_{24}\cdot 4H_2O$ was added to an aqueous solution containing ferric nitrate ($Fe(NO_3)_3\cdot 9H_2O$) and magnesium nitrate ($Mg(NO_3)_2\cdot 6H_2O$) in a Pyrex dish, keeping the molar ratio of Mo:Fe:MgO at 0.1:0.9:13. To this mixture was added an appropriate amount of urea (three times the stoichiometric ratio), which acts as the fuel in the combustion process. The mixture was dissolved by using a minimum amount of distilled water and kept in an oven at 70 °C for 12 h. The Pyrex dish containing the solution was placed in a furnace preheated at 550 °C. The thick orange-red solution immediately started boiling and underwent dehydration. The resulting thick paste frothed and blazed with a white flame, with the production of a light material which then swelled to the capacity of the Pyrex dish. The total combustion process was over in 10 min. The combustion product was baked at 550 °C for 3 h and ground to a fine powder. Preparation of the catalyst by conventional methods, such as wet impigration or coprecipitation, yields inhomogeneous catalyst particles, whereas the combustion route employed here gives homogeneous catalyst particles.

For obtaining nitrogen-doped DWNTs, the procedure was similar to that used for undoped DWNTs, expect that ammonia or pyridine vapor was taken in mixture with CH_4.[16] For doping nitrogen by using ammonia, the supported Fe−Mo catalyst (200 mg) was placed in a quartz boat at the center of the quartz reactor tube. The quartz tube was heated to 950 °C in an Ar atmosphere. Subsequently, CH_4 (50 sccm), NH_3 (5 sccm), and Ar (150 sccm) were mixed and introduced at the inlet of the reactor tube. After 20 min, the reactor was cooled to room temperature in an Ar atmosphere. For N-doping using pyridine, the supported Fe−Mo catalyst (200 mg) was placed in a quartz boat at the center of the quartz reactor tube. The quartz tube was heated to 950 °C in an Ar atmosphere. Subsequently, 40 sccm of CH_4 was passed through a bubbler containing pyridine, which carries the pyridine vapor to the furnace. These vapors were mixed with 150 sccm of Ar and passed over the MgO-supported catalyst, maintained at 950 °C for 20 min.

For the synthesis of boron-doped DWNTs, diborane (B_2H_6) was used as the boron source, the rest of the procedure being similar to that for undoped DWNts. B_2H_6 vapor was generated by the addition of BF_3−diethyl etherate to sodium borohydride in tetraglyme.[18] Fifty sccm of CH_4 was mixed and passed along with B_2H_6 vapors. These vapors were further mixed along with 150 sccm of Ar and passed over the MgO-supported catalyst powder, maintained at 950 °C for 20 min.

The percentage of DWNTs in all our preparations was 90% or higher. Such high preferential yields of DWNTs have been reported in the literature.[9,10] In order to dissolve the metal nanoparticles in the DWNTs, the as-prepared nanotubes were treated with concentrated HCl at 60 °C for 24 h. The product was washed with distilled water, dried, dispersed in ethanol under sonication, and filtered using Millipore (0.2 μm) filter paper. The filtered product was dried in an oven at 100 °C for 2 h and heated to 850 °C in a furnace at a rate of 3 °C per minute in flowing hydrogen at 100 sccm and held at that temperature for 6 h to remove the amorphous carbon present on the nanotube walls.[32] The resulting sample was again stirred in concentrated HCl at 60 °C for 3 h and heated in a furnace at 850 °C for 6 h in flowing hydrogen (100 sccm). The same procedure was employed to purify doped DWNTs, except that dilute HCl was used instead of concentrated HCl. It must be noted that hydrogen treatment at high temperatures has been found to be a very good method to eliminate amorphous carbon present on the carbon nanotubes.[32]

We have characterized the undoped and doped DWNTs by various techniques. Field emission scanning electron microscope (FESEM) images were recorded with a FEI NOVA NANOSEM 600. UV–vis absorption spectra of the nanotubes were recorded using a Perkin-Elmer Lambda 900 UV/vis/NIR spectrometer. Thermogravimetric analysis was carried out using a Mettler Toledo TGA 850 instrument. Raman spectra were recorded with a LabRAM HR high-resolution Raman spectrometer (Horiba Jobin Yvon) using a He−Ne laser ($\lambda = 630$ nm). Transmission electron microscope images were obtained with a JEOL JEM 3010 instrument. X-ray photoelectron spectroscopy was recorded using a VG scientific ESCA Laboratory V spectrometer. EELS were recorded with a transsmision electron microscope (FEI, TECNAI F30) equipped with an energy filter for EELS operating at 300 kV.

Acknowledgment. L.S.P. acknowledges CSIR, New Delhi, for a junior research fellowship.

REFERENCES AND NOTES

1 Dai, H.; Rinzler, A.; Nikolaev, P.; Thess, A.; Colbert, D.; Smalley, R. Single-Wall Nanotubes Produced by Metal-Catalyzed Disproportionation of Carbon Monoxide. *Chem. Phys. Lett.* **1996**, *260*, 471–475.

2 Rao, C. N. R.; Govindaraj, A. *Nanotubes and Nanowires*; RSC Nanoscience & Nanotechnology Series; RSC Publishing: Cambridge, UK, 2005.

3 Kurachi, H.; Uemura, S.; Yotani, J.; Nagasako, T.; Yamada, H.; Ezaki, T.; Maesoba, T.; Loutfy, R.; Moravsky, A.; Nakazawa, T.; Saito, Y. Proceedings of the 21st International Display Research Conference in conjunction with the 8th International Display Workshops, 2001; pp 1237−1240.

4 Saito, R.; Matsuo, R.; Kimura, T.; Dresselhaus, G.; Dresselhaus, M. S. Anomalous Potential Barrier of Double-Wall Carbon Nanotube. *Chem. Phys. Lett.* **2001**, *348*, 187–193.

5 Sugai, T.; Yoshida, H.; Shimada, T.; Okazaki, T.; Shinohara, H. New Synthesis of High-Quality Double-Walled Carbon Nanotubes by High-Temperature Pulsed Arc Discharge. *Nano Lett.* **2003**, *3*, 769–773.

6 Lee, Y. D.; Lee, H. J.; Han, J. H.; Yoo, J. E.; Lee, Y.-H.; Kim, J. K.; Nahm, S.; Ju, B.-K. Synthesis of Double-Walled Carbon Nanotubes by Catalytic Chemical Vapor Deposition and Their Field Emission Properties. *J. Phys. Chem. B* **2006**, *110*, 5310–5314.

7 Liu, B. C.; Lyu, S. C.; Lee, T. J.; Choi, S. K.; Eum, S. J.; Yang, C. W.; Park, C. Y.; Lee, C. J. Synthesis of Single- and Double-Walled Carbon Nanotubes by Catalytic Decomposition of Methane. *Chem. Phys. Lett.* **2003**, *373*, 475–479.

8 Lyu, S. C.; Lee, T. J.; Yang, C. W.; Lee, C. J. Synthesis and Characterization of High-Quality Double-Walled Carbon Nanotubes by Catalytic Decomposition of Alcohol. *Chem. Commun.* **2003**, *1404*, 1405.

9 Lyu, S. C.; Liu, B. C.; Lee, S. H.; Park, C. Y.; Kang, H. K.; Yang, C.-W; Lee, C. J. Large-Scale Synthesis of High-Quality Double-Walled Carbon Nanotubes by Catalytic Decomposition of n-Hexane. *J. Phys. Chem. B* **2004**, *108*, 2192–2194.

10 Lyu, S. C.; Liu, B. C.; Lee, C. J.; Kang, H. K.; Yang, C-W; Park, C. Y. High-Quality Double-Walled Carbon Nanotubes Produced by Catalytic Decomposition of Benzene. *Chem. Mater.* **2003**, *15*, 3951–3954.

11 Wei, J.; Ci, L.; Jiang, B.; Li, Y.; Zhang, X.; Zhu, H.; Xua, C.; Wua, D. Preparation of Highly Pure Double-Walled Carbon Nanotubes. *J. Mater. Chem.* **2003**, *13*, 1340–1344.

12 Ren, W.; Cheng, H.-M. Aligned Double-Walled Carbon Nanotube Long Ropes with a Narrow Diameter Distribution. *J. Phys. Chem. B* **2005**, *109*, 7169–7173.

13 Hassanien, A.; Tokumoto, M.; Kumazawa, Y.; Kataura, H.; Maniwa, Y.; Suzuki, S.; Achida, Y. Atomic Structure and Electronic Properties of Single-Wall Carbon Nanotubes Probed by Scanning Tunneling Microscope at Room Temperature. *Appl. Phys. Lett.* **1998**, *73*, 3839–3841.

14 Sen, R.; Satishkumar, B. C.; Govindaraj, A.; Harikumar, K. R.; Renganathan, M. K.; Rao, C. N. R. Nitrogen-Containing Carbon Nanotubes. *J. Mater. Chem.* **1997**, *7*, 2335–2337.

15 Sen, R.; Satishkumar, B. C.; Govindaraj, A.; Harikumar, K. R.; Raina, G.; Zhang, J.-P.; Cheetham, A. K.; Rao, C. N. R. B-C-N, C-N and B-N Nanotubes Produced by the Pyrolysis of Precursor Molecules over Co Catalysts. *Chem. Phys. Lett.* **1998**, *287*, 671–676.

16 Nath, M.; Satishkumar, B. C.; Govindaraj, A.; Vinod, C. P.; Rao, C. N. R. Production of Bundles of Aligned Carbon and Carbon-Nitrogen Nanotubes by the Pyrolysis of

Precursors on Silica-Supported Iron and Cobalt Catalysts. *Chem. Phys. Lett.* **2000**, *322*, 333–340.
17 Villalpando-Paez, F.; Zamudio, A.; Elias, A. L.; Son, H.; Barros, E. B.; Chou, S. G.; Kim, Y. A.; Muramatsu, H.; Hayashi, T.; Kong, J.; *et al.* Synthesis and Characterization of Long Strands of Nitrogen-Doped Single-Walled Carbon Nanotubes. *Chem. Phys. Lett.* **2006**, *424*, 345–352.
18 Satishkumar, B. C.; Govindaraj, A.; Harikumar, K. R.; Zhang, J.-P; Cheetham, A. K.; Rao, C. N. R. Boron-Carbon Nanotubes from the Pyrolysis of C_2H_2-B_2H_6 Mixtures. *Chem. Phys. Lett.* **1999**, *300*, 473–477.
19 McGuire, K.; Gothard, N.; Gai, P. L.; Dresselhaus, M. S.; Sumanasekera, G.; Rao, A. M. Synthesis and Raman Characterization of Boron-Doped Single-Walled Carbon Nanotubes. *Carbon* **2005**, *43*, 219–227.
20 Charlier, J.-C.; Terrones, M.; Baxendale, M.; Meunier, V.; Zacharia, T.; Rupesinghe, N. L.; Hsu, W. K.; Grobert, N.; Terrones, H.; Amaratunga, G. A. J. Enhanced Electron Field Emission in B-doped Carbon Nanotubes. *Nano Lett.* **2002**, *2*, 1191–1195.
21 Sharma, R. B.; Late, D. J.; Joag, D. S.; Govindaraj, A.; Rao, C. N. R. Field Emission Properties of Boron and Nitrogen Doped Carbon Nanotubes. *Chem. Phys. Lett.* **2006**, *428*, 102–108.
22 Czerw, R.; Terrones, M.; Charlier, J.-C.; Blase, X.; Foley, B.; Kamalakaran, R.; Grobert, N.; Terrones, H.; Tekleab, D.; Ajayan, P. M.; *et al.* Identification of Electron Donor States in N-Doped Carbon Nanotubes. *Nano Lett.* **2001**, *1*, 457–460.
23 Kim, S. Y.; Lee, J.; Na, C. W.; Park, J.; Seo, K.; Kim, B. N-Doped Double-Walled Carbon Nanotubes Synthesized by Chemical Vapor Deposition. *Chem. Phys. Lett.* **2005**, *413*, 300–305.
24 Dresselhaus, M. S.; Eklund, P. C. Phonons in Carbon Nanotubes. *Adv. Phys.* **2000**, *49*, 705–814.
25 Yang, Q. H.; Hou, P. X.; Unno, M.; Yamauchi, S.; Saito, R.; Kyotani, T. Dual Raman Features of Double Coaxial Carbon Nanotubes with N-Doped and B-Doped Multiwalls. *Nano Lett.* **2005**, *5*, 2465–2469.
26 McGuire, K.; Gothard, N.; Gai, P. L.; Dresselhaus, M. S.; Sumanasekera, G.; Rao, A. M. Synthesis and Raman Characterization of Boron-Doped Single-Walled Carbon Nanotubes. *Carbon* **2005**, *43*, 219–227.
27 Das, A.; Sood, A. K.; Govindaraj, A.; Saitta, A. M.; Lazzeri, M.; Mauri, F.; Rao, C. N. R. Doping in Carbon Nanotubes Probed by Raman and Transport Measurements. *Phys. Rev. Lett.* **2007**, *99*, 136803 (1–4).
28 Li, F.; Chou, S. G.; Ren, W.; Gardecki, J. A.; Swan, A. K.; Unlu, M. S.; Goldbeg, B. B.; Cheng, H.-M.; Dresselhaus, M. S. Identification of the Constituents of Double-Walled Carbon Nanotubes using Raman Spectra Taken with Different Laser-Excitation Energies. *J. Mater. Res.* **2003**, *18*, 1251–1258.
29 Kishi, N.; Kikuchi, S.; Ramesh, P.; Sugai, T.; Watanabe, Y.; Shinohara, H. Enhanced Photoluminescence from Very Thin Double-Wall Carbon Nanotubes Synthesized by the Zeolite-CCVD Method. *J. Phys. Chem. B* **2006**, *110*, 24816–24821.
30 Patil, K. C. Advanced Ceramics: Combustion Synthesis and Properties. *Bull. Mater. Sci.* **1993**, *16*, 533–541.
31 Flahaut, E.; Peigney, A.; Bacsa, W. S.; Bacsa, R. R.; Laurent, C. CCVD Synthesis of Carbon Nanotubes from (Mg,Co,Mo)O Catalysts: Influence of the Proportions of Cobalt and Molybdenum. *J. Mater. Chem.* **2004**, *14*, 646–653.
32 Vivekchand, S. R. C.; Govindaraj, A.; Motin Seikh, Md.; Rao, C. N. R. New Method of Purification of Carbon Nanotubes Based on Hydrogen Treatment. *J. Phys. Chem. B* **2004**, *108*, 6935–6937.